HHS Public Access

Author manuscript

Drug Deliv. Author manuscript; available in PMC 2016 September 01.

Published in final edited form as:

Drug Deliv. 2016 March ; 23(3): 968–980. doi:10.3109/10717544.2014.923068.

Formulation development of a novel targeted theranostic nanoemulsion of docetaxel to overcome multidrug resistance in ovarian cancer

Srinivas Ganta[1], **Amit Singh**[2], **Yashesh Rawal**[3], **Joseph Cacaccio**[1,3], **Niravkumar R. Patel**[1], **Praveen Kulkarni**[4,5], **Craig F. Ferris**[4,5], **Mansoor M. Amiji**[2,5], and **Timothy P. Coleman**[1,3,5,6]

[1]Nemucore Medical Innovations, Inc., Worcester, MA, USA

[2]Department of Pharmaceutical Sciences, School of Pharmacy, Northeastern University, Boston, MA, USA

[3]Blue Ocean Biomanufacturing, Inc., Worcester, MA, USA

[4]Center for Translational Imaging, Northeastern University, Boston, MA, USA

[5]Center for Translational Cancer Nanomedicine Northeastern University, Boston, MA, USA

[6]Foundation for the Advancement of Personalized Medicine Manufacturing, Phoenix, AZ, USA

Abstract

Objective—Ovarian cancer is a highly lethal disease in which the majority of patients eventually demonstrate multidrug resistance. Develop a novel active targeted theranostic nanomedicine designed to overcome drug efflux mechanisms, using a Generally Regarded As Safe (GRAS) grade nanoemulsion (NE) as a clinically relevant platform.

Materials and methods—The NEs surface-functionalized with folate and gadolinium, were made using GRAS grade excipients and a high-shear microfluidization process. Efficacy was evaluated in ovarian cancer cells, SKOV3 and SKOV3TR. The NE accumulation in tumors was evaluated in SKOV3 tumor-bearing mice by magnetic resonance imaging (MRI).

Results and discussion—The NE with particle size <150nm were stable in plasma and parenteral fluids for 24 h. Ovarian cancer cells *in vitro* efficiently took up the non-targeted and folate-targeted NEs; improved cytotoxicity was observed for the folate-targeted NEs showing a 270- fold drop in the IC_{50} in SKOV3TR cells as compared to docetaxel alone. The addition of gadolinium did not affect cell viability *in vitro*, but showed relaxation times comparable to Magnevist®. Folate-targeted NEs accumulated in tumors for prolonged period of time compared to Magnevist® and showed enhanced contrast compared to non-targeted NEs with MRI in SKOV3 tumor-bearing mice suggesting active targeting of NEs due to folate modification.

Address for correspondence: Timothy P. Coleman, PhD, CEO & President, Nemucore Medical Innovations, Inc., Worcester, MA 01608, USA. tcoleman@nemucore.com.

Declaration of interest

Research reported in this publication was supported by the National Cancer Institute of the National Institutes of Health under Awards Number R01CA158881 and Number U54 CA151881. The content is solely the responsibility of the authors and does not necessarily represent the official views of the National Institutes of Health. The authors report no conflicts of interest.

Conclusions—A folate-targeted, theranostic NE delivers docetaxel by receptor mediated endocytosis that shows enhanced cytotoxicity capable of overcoming ABC transporter mediated taxane resistance. The diagnostic capability of the targeted nanomedicine showed enhanced contrast in tumors compared to clinically relevant MRI contrast agent Magnevist®.

Keywords

Docetaxel; folate; gadolinium; MRI

Introduction

Taxane chemotherapies are important primary (e.g. paclitaxel) and secondary (e.g. docetaxel) line of treatment for ovarian cancer patients. Even with these powerful chemotherapies eventually all patients become resistant to treatment, clinically defined as multidrug resistance (MDR). Factors leading to MDR can include enzymatic inactivation, ATP binding cassette (ABC) transporters (i.e. P-glycoprotein (P-gp) and breast cancer resistant protein (BRCP-1)) responsible for drug efflux mechanisms, or dysregulation of DNA repair mechanisms. Drug efflux inhibitors like PSC 833, GF120918, VX-710, LY335979, OC144093 and XR9576 have been clinically investigated to mitigate drug efflux mechanisms but have shown limited benefits and none have yet been approved by the U.S. Food and Drug Administration (FDA) for clinical use (Seiden et al., 2002; Pusztai et al., 2005; Ruff et al., 2009). These compounds were designed as inhibitors of ABC transporters to physically block drug efflux. Unlike these pharmacological means the development of nanomedicines can integrate design features which take advantage of simultaneous delivery of drug efflux counter measures while transporting a clinically relevant chemotherapeutic payload. Instead of pharmacologically blocking ABC transporters (Kelly et al., 2011), a folate-targeted nanoemulsion (NE) was designed to utilize receptor-mediated endocytosis to deliver docetaxel (DTX). Receptor-mediated endocytosis has been proposed as a means to bypass ABC transporter mediated drug efflux (Goren et al., 2000). Folate was chosen as the ligand because folate receptor (FR) is poorly expressed or absent on most normal tissues (Leamon, 2008). However, it is over-expressed in many cancers and is highly relevant in epithelial ovarian cancer as ~80% express FR (Toffoli et al., 1997; Sudimack & Lee, 2000; Li et al., 2009; Spannuth et al., 2010).

In this study, we have investigated the development of a folate-targeted theranostic NE, annotated with the clinically relevant MRI contrast agent Gd and carrying DTX for the enhancement of cytotoxicity in SKOV3 and SKOV3TR, taxane sensitive and resistant respectively. NEs have proven to be a versatile platform for the development of a variety of drug delivery vehicles (Ganta et al., 2014a,b). For heavily treated patients, in the later stages of a diagnosis, time to ascertain if a therapy is working is of up most importance. Therefore, drug distribution is an important parameter to understand, so the NE designed were optimized to carry the MRI imaging agent Gd to act as a surrogate marker for drug distribution. In addition to formulation optimization, we examined intracellular delivery, ability to change apoptotic potential, reversal of taxane resistance, and capacity to be an MRI agent.

Materials and methods

Materials

DTX was obtained from LC Laboratories (Woburn, MA). L-α-phosphatidylethanolamine transphosphatidylated (PE) and C6-NBD-ceramide were purchased from Avanti Polar Lipids (Alabaster, AL). Egg phosphotidylcholine (Lipoid® E80) was received from Lipoid GmbH (Ludwigshaffen, Germany). 1,2- distearoyl-sn-glycero-3-phosphoethanolamine- N-[methoxy-(polyethyleneglycol)-2000] (DSPEPEG$_{2000}$) and 1,2-distearoyl-sn-glycero- 3-phosphoethanolamine- N-[maleimide(polyethylene glycol)-2000] (ammonium salt) (DSPE-PEG$_{2000}$-MAL) was purchased from Laysan Bio Inc., (Arab, AL) Poly unsaturated fatty acid (PUFA) rich flaxseed oil was obtained from Puritan's Pride Inc. (Oakdale, NY). Cysteine, folic acid (FA), diethylenetriaminepentaacetic dianhydride (DTPA), 2,7-bis(*o*-arsenophenylazo)- 1,8-dihydroxynaphthalene-3,6-disulfonic acid (arsenazo III), 3-[4,5-dimethyl thiazolyl]-2,5-diphenyl tetrazolium bromide (MTT reagent), gadolinium (III) chloride ($GdCl_3$) hexahydrate, pyridine, ninhydrine, and N,N′-dicyclohexylcabodiimide (DCC) were obtained from Sigma Chemicals (St. Louis, MO). Apo-ONE® Homogeneous Caspase-3/7 assay was obtained from Promega (Madison, WI). Slowfade® Gold Antifade mounting media supplemented with DAPI, lyso-tracker red, Novex® 4–12% Tri-glycine mini gels and PVDF membrane were obtained from Life Technologies (Grand Island, NY). RIPA cell lysis buffer, Halt™ protease inhibitor cocktail, Pierce™ Lane Marker Sample Buffers, Running buffer (10X), NuPAGE® transfer buffer and SuperSignal West Pico Chemiluminescent Substrate were obtained from Fisher Scientific (Pittsburgh, PA). Anti-P-gp mouse 1 ° antibody (ab80594), anti β-actin mouse 1 ° antibody (ab8224), and HRP-linked 2 ° antibody (Goat anti mouse IgG, ab97023) were obtained from Abcam (Cambridge, MA). All other chemicals and solvents used were of the highest available grade.

SKOV3 human ovarian carcinoma cells were purchased from ATCC (Manassas, VA). Multi-drug resistant SKOV3TR cells were generously provided by Dr. Duan Zhenfeng (Mass General Hospital, Boston, MA).

Synthesis of folate-PEG-DSPE

DSPE-PEG$_{2000}$-MAL (200 mg) was added to cysteine (Cys) (16.5 mg) dissolved in 1M HEPES buffer (pH 7.4) at 1:2 molar ratio and mixed under nitrogen environment at 4 °C for overnight to facilitate to conjugation. The DSPE-PEG$_{2000}$-Cys conjugate was purified by dialysis against water using dialysis bag with molecular weight cut-off of 3500 Da (Spectrapore, Spectrum Laboratories, CA) and lyophilized. DSPE-PEG2000- Cys (120 mg) was dissolved in 12ml dry DMSO and 13 mg of FA was added to it. A 7 ml of pyridine and 16 mg of DCC was added subsequently and the mixture stirred for 4 h at room temperature to allow amide coupling of FA to the amine group of Cys. The final product was dialyzed in water for 24 h, lyophilized and analyzed by NMR to confirm conjugation.

Synthesis of Gd-DTPA-PE

Gd-DTPA-PE was synthesized as reported earlier with modifications (Levchenko et al., 2002). L-α-phosphatidylethanolamine transphosphatidylated (PE) (100 mg) dissolved in

chloroform (4 ml) was treated with triethylamine (30 μl). This solution was added drop-wise to DTPA (400 mg) dissolved in DMSO (20 ml), and the mixture was stirred for 3 h under nitrogen atmosphere at room temperature. Chloroform was removed by blowing nitrogen, and reaction was incubated overnight at RT. The resulting DTPA-PE conjugate was purified by dialysis (6–8000 Da, Spectrapore, Spectrum Laboratories, CA) against 5% DMSO in water at room temperature for 24 h followed by further 24 h of dialysis in water. The purified sample was lyophilized and the purity of DTPA-PE complex was determined by thin layer chromatography (TLC) using a mobile phase of chloroform, methanol and water at 65:25:4 (v/v) ratio, and ninhydrin as visualizing reagent. In the next step, Gd was chelated to DTPA by adding 18.5 mg of $GdCl_3$ to DTPA-PE complex in 20ml of DMSO and the reaction mixture stirred for 1 h. The resulting Gd-DTPA-PE conjugate was purified by dialysis against water at room temperature for 24 h. The purified sample was lyophilized and stored at −20 °C until use.

Preparation of the NE formulations

Oil-in-water NE formulation encapsulating DTX was prepared by high shear homogenization method using LV1 Microfluidizer (Microfluidics Corporation, Newton, MA). DTX (10 mg) dissolved in chloroform was added to flaxseed oil (1 g) and chloroform evaporated using nitrogen gas, resulting in formation of oil phase. The aqueous phase of the formulation was prepared by dissolving egg lecithin (120 mg) and DSPE-PEG_{2000} (15 mg) in 4ml of glycerol (2.21% w/v)-water. To this initial solution, Gd-DTPA-PE (100 mg) and folate conjugate (8 mg) were added and stirred for 2 h to achieve complete dissolution of all components. After this, aqueous and oil phases were heated (60 °C, 2 min), mixed and homogenized at 25 000 psi for 10 cycles to obtain the NE formulation. Non-targeted formulation (DTX-NE NT) without a folate conjugate and corresponding blank NEs without the DTX were prepared in a similar manner. Additionally, non-targeted and folate targeted NEs for fluorescent microscopy were prepared in a similar manner by replacing DTX with a fluorescent labeled ceramide, C6-NBD-ceramide.

Formulation characterization

Particle size and zeta potential analysis—Size distribution and zeta potential were measured by diluting 10 μl of the different NE formulations in 10 ml of DI water and subjected to analysis using Zetas Sizer ZS (Malvern, Worcestershire, UK). The average droplet size was measured for each nanoemulsion formulation by dynamic light scattering at room temperature and a 90 ° fixed angle. The hydrodynamic radius and poly-dispersity index (PDI) of the droplets were determined for a count rate between 100–500 kcps. For zeta potential measurements, diluted sample was placed in electrophoretic cell and charge was recorded.

Transmission electron microscopy (TEM)—Samples for TEM analysis were prepared by dispersing 2 μl of the NE in 10 ml of DI water. From these diluted samples, 10 μl was drop-coated on the Formvar-coated copper grids (Electron Microscopy Science, Hatfield, PA) and allowed to stand for 1 min following which, excess was drained using Whatman filter paper. The NE were then stained with 10 μL of 1% (w/v) uranyl acetate for 1 min, excess stain was removed using Whatman filter paper. The grids were allowed to air-dry

before performing observation under a JEOL 100X transmission electron microscope (Peabody, MA).

Analysis of DTX loading and encapsulation—A high-performance liquid chromatography (HPLC) assay was performed to measure DTX loading and encapsulation efficiency of the NEs. A Waters LC system (model 2487, Waters Corporation, Milford) comprising of a quaternary pump, an autosampler, and UV-detector was used for the analysis. The LC system was interfaced with Empower 3 software for remote controlling, data acquisition and processing. The mobile phase consisted of acetonitrile:water (50:50 v/v) and was pumped to a reverse phase C_{18} column (4.6mm×15 mm, 5 μm, Hypersil Gold, US) with a C_{18} pre-column (4mm×20 mm, 5 μm, Phenomenex, US) at a flow rate of 1 ml/min. Samples at 10 μl were injected and monitored for DTX elution at 230 nm.

Both non-targeted and folate-targeted NEs were assayed for DTX loading prior to all studies. A standard curve of DTX was generated with a linear range of detection between 0.1–50 μg/ml. To determine loading efficiency, a 10 μl formulation was diluted in 1ml of acetonitrile, vortexed and centrifuged at 10 000 rpmfor 15 min. The supernatant was subjected to HPLC analysis to determine concentration of DTX.

DTX encapsulation efficiency in the NE was determined by an ultracentrifugation method using centrifugal filter devices (MWCO 3,000 Da; centricorn, Millipore, MA). one ml of the nanoemulsion was placed in the upper donor chamber, centrifuged at 10 000 rpm for 30 min to separate the aqueous phase in to the recovery chamber and the sample containing the drug was collected from the donor chamber. The DTX concentration in the recovery and donor chambers was measured by HPLC and% encapsulation was calculated.

Gadolinium assay—Arsenazo III was employed to determine free Gd content during Gd-DTPA-PE synthesis as described previously (8,9). Samples assayed for free Gd were prepared by mixing of 50 μl sample with 100 μl of 0.2mM arsenazo III solution and diluted to 1ml with water. Then 200 μl aliquots of these samples were added to 96-well plate and read at 652 nm on Synergy HT plate reader (BioTex). A standard curve of Gd was prepared using $GdCl_3$ with the linearity range of 2–50 μg/ml and used for calculating Gd amount in the samples.

T1 relaxivities—Gd-annotated NE samples were filled in tubes and ran through a phantom Brucker 500 MHz MRI machine (Bruker Biospec 20/70, Bruker Biospin MRI, Inc) in a 4.7 Tesla magnetic field, giving MRI scans showing NE generated contrast as well as T1 time measurements. Magnevist®, a clinically used Gd-DTPA chelate also tested for T1 relaxation time at same Gd concentration as Gd-annotated NEs.

DTX release from NEs—The DTX release assays were carried out by loading NE formulations equivalent to 4mg of DTX into dialysis bag (3500 Da) and placing it in 100 ml release media (0.5% Tween 80/PBS, pH 7.4) maintained at 37 °C and stirring rate of 400 rpm. Sample aliquots (1 ml) were collected at different time intervals up to 72 h and replaced with fresh media. The docetaxel concentration in the samples was analyzed using HPLC as described above. At the end of study, unreleased drug remained in the dialysis bag

was measured and compared with the release data. The cumulative amount of DTX released and release kinetics were calculated to assess the release profile.

Stability of formulations in plasma and intravenous infusion solutions—NEs were diluted in dog plasma and electrolyte solutions, and monitored for particle size over 24 h at 37 °C. The change in particle size was used as indicator of stability upon dilution. For this, NEs were diluted 90% with fresh dog plasma, sodium chloride (0.9%), dextrose (5%) and phosphate buffered saline (PBS pH 7.4) and incubated at 37 °C. Aliquots of 10 μl of samples were taken for analysis at 1, 2, 4, 6, 8 and 24 h, diluted 1000-fold with distilled water and analyzed particle size using Zetasizer ZS as described above.

In vitro studies

Cell culture conditions—SKOV3 and SKOV3TR cells were cultured in RPMI 1640 media supplemented with 10% fetal bovine serum and 1% Penicillin/streptomycin and maintained in a humidified 95% O_2/5% CO_2 atmosphere at 37 °C. Cells were grown until 60–70% confluent in the flasks and trypsinized with a solution 0.25% Trypsin with 2.25mM EDTA in HBSS. Trypan blue exclusion method was employed to determine the viable cells.

Cellular uptake—SKOV3 cells were seeded in 6-well plate over cover slip at density of 100 000 cells/well and incubated for 24 h before treatment. Cells were washed with media and incubated with either non-targeted or folate-targeted C6-NBD-ceramide labeled NEs for 5, and 15 minutes, followed by washing with PBS. Cells were incubated with lysotracker red according to manufacturer's protocol for 20 minutes followed by treatment with 4% formaldehyde for 30 minand mounted on to a glass slide with a Slowfade® Gold Antifade mounting media supplemented with DAPI. Glass slides were rested for 30 minutes on flat surface in dark before imaging localization of fluorescence signal using Zeiss confocal microscope (LSM-700).

P-gp expression by western blot analysis—SKOV3 and SKOV3TR cells were grown in T75 flask until 80% confluent. Cells were mechanically scraped and centrifuged to get cell pellet. Cells were lysed in 200 μl of radioimmunoprecipitation assay (RIPA) cell lysis buffer with Halt™ protease inhibitor cocktail for 30 minutes on ice. Cell lysate was centrifuged at 13,000 rpm for 15 minutes and supernatant was analyzed using bicinchoninic acid (BCA) assay for protein concentration. Loading buffer with reducing agent was added to cell lysate containing 20 μg of protein and final volume of 25 μl was achieved by diluting using PBS. These samples were heated at 85 °C for 5 minutes and loaded in gel locked in XCell SureLock™ system with running buffer in place as described by manufacturer. Samples were electrophoresed on a 4–12% SDS-PAGE. Proteins were transferred on to PVDF membrane using transfer assembly in XCell SureLock™ system. Transfer sandwich was prepared by placing from anode sponge, sponge, filter paper, gel, PVDF, filter paper, sponge and sponge to cathode. PVDF membrane was then incubated in blocking buffer in 1X tris buffered saline with Tween 20 (TBST) (1% BSA) for 1 h followed by incubation with 1 μg/ml of primary antibody (mouse anti P-gp primary antibody, AB80594) overnight at 4 °C. Membrane was washed three times with TBST for 5 minwith rocking followed by incubation with secondary antibody (HRP-linked Goat anti mouse IgG, AB97023) for 1 h in

1%BSA in TBST at room temperature. Membrane was washed again three times as described before followed by incubation with 10 ml of chemiluminescence substrate (SuperSignal West Pico Kit, Pittsburgh, PA) for 5 min. Substrate was discarded and membrane was placed in plastic bag before detecting luminescence using KODAK 2000R (Carestream, Rochester, NY) imaging system using cooled CCD camera. β-actin was used as loading control for each sample.

Cytotoxicity assay—SKOV3 and SKOV3TR cells were seeded in 96-well plate at 3000 cells per well. After 24 h seeding, cells were treated with concentrations of DTX over eight orders of magnitude ranging from 0.001nM to 100 000 nM. For this, DTX solution in DMSO, non-targeted and folate-targeted NEs were diluted in RPMI media and added to cells. After the 72 h treatment, cells were washed with media and incubated with MTT reagent (50 μg/well) for 3 h. RPMI growth media was used as a negative control (0% cell death) and poly (ethyleneimine), a cationic cytotoxic polymer at a concentration of 250 μg/ml (molecular weight 10 kDa) was used as a positive control (100% cell death). Vehicle controls without any drug were also employed at corresponding volumes. Dose-response curves and IC_{50} values were obtained by fitting data Sigmoidal-dose response curves using Graphpad Prism 5.

Caspase-3/7 activity—SKOV3 and SKOV3TR cells were seeded in 96-well plate at 2000 cells/well and incubated for 24 h before treatment. Cells were then treated with either DTX solution in DMSO, nontargeted and folate-targeted NEs at 1 nM DTX for SKOV3 cells and 100nM DTX for SKOV3TR cells for 1, 2, 4, and 8 h. Media with caspase reagent without cells and untreated cells were kept as control. Additionally, vehicle controls were employed to account for any caspase activity. After desired incubation, cells were washed with media followed by incubation with 50 μl of caspase 3/7 activity assay reagent mixed with 50 μl of complete media according to manufacturer's protocol. Cells were incubated for 2 h and fluorescence was measured at 499 nm excitation and 521 nm emission. Fold change in caspase 3/7 activation by DTX when delivered using DMSO, non-targeted or folate-targeted NEs was calculated after subtracting background fluorescence (media+assay reagent without cells) from all reading.

In vivo studies

T1 weighted MRI imaging—SKOV3, approximately 1×10^6 cells suspended in PBS: Matrigel (1:1), were injected subcutaneously in female nu/nu mice. Tumors were allowed to grow until $250mm^3$. Mice were pretreated with 400 μg of Pemetrexed 1 h prior to imaging agent administration. Three mice per cohort were then injected with either magnevist, NT-unloaded NEs, or folate-targeted unloaded NEs at final concentration of Gd at 0.072 mmoles/kg. The mice were anesthetized with isoflurate during scans and were kept in MRI between scans. T1 weighted images were acquired using a phantom Brucker 500 MHz MRI machine (Bruker Biospec 20/70, Bruker Biospin MRI, Inc, Billerica, MA) in a 4.7 Tesla magnetic field up to 24 h.

Data analysis

Data are reported as the average and standard deviation. Comparisons between the groups were made using student's t-test and with more than two groups, the ANOVA test was used. Values of $p<0.05$ were considered statistically significant.

Results

Characterization of the conjugates

NMR spectroscopy was used to characterize all the individual components and the final purified folate-PEG-DSPE conjugate to confirm the final product (Figure 1). The proton signature from pure DSPE-PEG-Mal and folic acid (Figures 1A and B, respectively) could be successfully assigned in the NMR spectra obtained and these spectra from standards were used to confirm successful formation of the folic acid conjugate. The NMR spectrum of folate-PEG-DSPE shows the signature peaks of PEG protons between 3.2–3.5 (Figure 1C, label b) and folic acid ring protons between 8–9 (Figure 1C, label c) corresponding to the peaks found in standards. Most importantly, a peak between 5–6 (Figure 1C, label a) corresponding to an integration value equivalent to three protons could be attributed to the three amide protons present in the conjugate, thereby confirming the successful formation of folic acid conjugate.

Conjugation of DTPA to PE was monitored by TLC where the appearance of a band at an Rf value of 0.4 confirmed the conjugation (Grant et al., 1989). The purified DTPA-PE conjugate was lyophilized and was further used for Gd chelation. Owing to toxicity associated with presence of free Gd, (Ersoy & Rybicki, 2007) it becomes pertinent to assess and remove any free Gd from the conjugate. Gd chelation to DTPA-PE was monitored colorimetrically by using 0.2mM solution of arsenazo III dye (Clogston & Patri, 2011). Arsenazo III binds with free metal ions forming a complex that can be colorimetrically detected but it does not interact with already complexed metal ions. Titration of the DTPA-PE conjugate with Gd ion using arsenazo III dye further enabled the confirmation of amount of Gd loading in the conjugate. The purified Gd-DTPA-PE conjugate was finally purified by dialysis, lyophilized and stored at −20 °C until used.

NE formulation and characterization

Blank, folate receptor-targeted blank, non-targeted drug-loaded and folate receptor- targeted drug-loaded NEs were prepared by a high-energy microfluidization process. Flaxseed oil, rich in polyunsaturated fatty acid (PUFA) such as omega-3 (linolenic acid) and omega-6 (linoleic acid), was used as oil phase of NE to dissolve DTX (Figure 2). Such PUFA rich oils not only enable loading a high concentration of lipophilic anti-cancer drug in to the formulation but also have been shown to possess cancer chemo-preventive attributes (Rose & Connolly, 1999). A series of formulation optimization studies were carried using different composition of oil, emulsifier and drug amount to develop a stable NE system with highest possible drug loading efficiency. The finally optimized NE composition consisted of flaxseed oil (20% w/v), egg phosphotidylcholine (lecithin) (2.4% w/v), $mPEG_{2000}$-DSPE or fol-PEG_{2000}-DSPE (0.3% w/v) and DTX (0.2% w/v). The blank NEs (non-targeted or targeted) consisted of the same components without the drug.

All the NE formulations were characterized for their size, surface charge, drug loading efficiency and T1 relaxivity values, which are summarized in Table 1. The average NE droplet hydrodynamic diameter was found to be in the range of 130–140 nm by dynamic light scattering (DLS) with a narrow polydispersity index (PDI), indicating that our production method yields uniform sized particles. Most importantly, a consistent size range for all the formulations suggest that incorporation of drug or targeting ligand does not impart any variation in the size of the NE droplet. Similarly, the average surface charge for all the NEs was around −50mV, suggesting that the addition of drug, MRI contrast agent or targeting ligand did not significantly alter the physical properties of the NEs (Table 1). The drug encapsulation capability of the NEs was assessed by an HPLC assay, which showed that all formulation were able to encapsulate DTX with 100% efficiency. This high efficiency of the drug encapsulation can be attributed to the lipophilic nature of DTX (LogP (6.55±0.73)), resulting in its retention in the oil core of the formulation. The DTX concentration in the final optimized NE formulation was 2 mg/ml.

T1 relaxivity of the formulations at 10, 1 and 0.1mM Gd concentration was measured using spin-echo sequence and the relaxation value was calculated by least-square fitting of the exponentially varying signal intensity as a function of recovery time. As shown in Table 1, the T1 relaxation time of the non-targeted nanoemulsion was found to be 35.51±13.5 and folate-targeted nanoemulsion was found to be 79.46± 2.63, and was comparable to that of Magnevist® (22±0.27 ms) at similar Gd concentrations. The physicochemical characterizations of all the formulations indicate that we could successfully prepare NE of identical size, charge, drug loading efficiency and T1 relaxivity with little inter-formulation variation.

Size and morphology of the blank, folate-targeted NE, non-targeted NE with DTX, and folate-targeted NE with DTX were analyzed by TEM show a spherical morphology with droplet size in the range of 100–120 nm, which is consistent with the size range obtained by DLS measurement (Figure 3). It is important to note that a decrease in the average particle size calculated by TEM compared to that obtained by DLS measurement is due to the fact that DLS analysis gives the hydrodynamic size of the oil droplets while TEM images show the actual size. Inset in each image in Figure 3 shows a particle size distribution plot calculated from a minimum of 30 NE droplets for the respective sample.

In vitro drug release analysis

The release profile of DTX from non-targeted and folate-targeted NE is shown in Figure 4. Both formulations release approximately 10% DTX at the end of 72 h. The DTX release data obtained were fitted into various kinetic models to describe the release kinetics as shown in Table 2. Predominant DTX release mechanism for non-targeted and folate-targeted NE formulations was zero order kinetics (Lachman et al., 1986).

Stability assessment of the NEs

Upon IV injection or mixing in parental infusion solutions, the physical stability of NE formulation can be affected ranging from particle aggregation and disruption. Aggregation leads to rapid *in vivo* clearance whereas particle disruption causes burst release kinetics of

payload (dose dumping). To test the NE formulations for stability, samples were diluted in plasma and parental infusion solutions and monitored for particle size over 24 h at 37 °C. The change in particle size was analyzed by DLS and used as indicator of stability upon dilution. For this, NE formulations were diluted Figure 5(A), 90% with fresh dog plasma, Figure 5(B), sodium chloride (0.9%), Figure 5(C), dextrose (5%) and Figure 5(D), phosphate buffered saline (PBS, pH 7.4) and incubated at 37 °C. The particle size did not change significantly over the period of 24 h indicating that both non-targeted and folate-targeted NE formulations were intact and, there was no particle aggregation and disruption in presence of high electrolyte concentration and plasma proteins. This data suggests that the NE formulations could be stable *in vivo* in blood circulation, show longer residence time, and increase tumor accumulation through the enhanced permeability and retention (EPR) effect.

Intracellular uptake with fluorescently labeled NEs

To determine the effect of folate-targeting, cellular uptake study was performed in folate-receptor positive SKOV3 cells. Cell nuclei and lysosomes were stained with DAPI and lysotracker red respectively. As can be seen in Figure 6, there is a time dependent uptake for non-targeted as well as folate-targeted NEs. However, higher uptake is observed in case of folate-targeted NE at 5 min time point compared to non-targeted NEs. The increased uptake of folate-targeted NE compared to non-targeted NE suggest involvement of folate receptors.

P-gp expression by western blot

P-gp expression was evaluated for SKOV3 and SKOV3TR cells as overexpression of this efflux pump results in drug resistance to DTX, the taxane used in the present study. In western blot analysis, overexpression of P-gp was detected in SKOV3TR, taxane resistant variant at 170 000 dalton whereas no P-gp expression was observed for SKOV3, taxanes sensitive cell line (Figure 7). β-actin was used as loading control and was observed for all three cell lines. These results demonstrate that the cell lines used in this study are ideal to investigate reversal of the multidrug resistance.

Cytotoxicity studies in sensitive and resistant ovarian cancer cells

In order to determine if the NEs produce a cytotoxic effect, the following experiments were done on SKOV3 and SKOV3TR cells. The data was obtained using a tetrazolium (MTT) assay, which measures the activity of cellular enzymes that reduces the MTT dye to its insoluble formazan. SKOV3TR cells express the ABC transporter, P-gp, which produces DTX efflux out of the cell and is associated with multidrug resistant cancer cells. The concentration required to inhibit growth of cells by 50% (IC_{50}) was calculated for each formulation and is shown in Table 3. As shown in Table 3, the IC_{50} of SKOV3 cells decreased 3.33-fold when DTX is encapsulated in folate-targeted NE formulation compared to DTX in solution. In taxane resistant SKOV3TR cells a 270- fold decrease in IC_{50} was observed when they were treated folate-targeted NE formulations when compared to DTX in solution. This significant improvement in cytotoxicity indicates that there is merit to the hypothesis that folate receptor mediated endocytosis is capable of bypassing multidrug

resistant mechanisms present in SKOV3TR. Nanoemulsion formulation containing no DTX did not affect cell viability.

Quantitative and qualitative apoptotic studies

In order to confirm that the anti-cancer activity of the nanoemulsion formulation is due to induction and upregulation of apoptotic pathways, the quantitative and qualitative apoptotic analysis was performed in SKOV3 cells. Figure 8 shows the caspase 3/7 activities in cells incubated with docetaxel in DMSO, non-targeted and folate targeted formulation as a function of time of incubation and the apoptotic activity was calculated relative to that obtained from untreated control cells. Figure 8(A) shows the apoptotic activity of the SKOV3 cells treated with DTX in different formulations for 1, 2 4 and 8 h. No significant change in apoptotic activity was observed post-incubation in the samples after 1 and 2 h but the apoptotic activity of the cells incubated with targeted NEs increased after 4 and 8 h suggesting that higher accumulation of the drug via receptor mediated uptake results in induction of apoptosis resulting in increased cell death compared to DTX in DMSO and non-targeted NE. This trend correlates well with *in vitro* cytotoxicity experiments where the targeted NE shows maximum cell-killing capability owing to an increased apoptosis induction.

The caspase 3/7 activities were similarly monitored in SKOV3TR cells treated with DTX in DMSO, non-targeted NE and folate-targeted NE for 2, 4 and 8 h (Figure 8B). Cells treated with DTX in DMSO, non-targeted nanoemulsion, and folate targeted nanoemulsion formulations for 2 h show essentially similar enzymatic activity with no significant difference. However, 4 h post-treatment with DTX containing formulations, cells start to show an enhanced caspase 3/7 activity with folate-targeted NE showing much higher increase (8-fold compared to untreated control) compared to non-targeted NE (6-fold) and taxotere (3.5-fold). The enzymatic activity for all the treatment groups decreased at 8 h incubation period with folate targeted nanoemulsion-treated cells still showing a significantly higher activity. This suggests that the enzymatic activity peaks around 4 h post-incubation in formulations. The significantly increased enzymatic activity in folate-targeted NE treated cells corroborate well with the cytotoxicity data where folate-targeted NE shows very-high cell-killing efficiency, which could be attributed to capability to induce apoptosis in the cells. It is also key to note that the levels of enzymatic activity is significantly higher in all the SKOV3TR cells (Figure 8B) compared to SKOV3 cells (Figure 8A) suggesting that even though these cells show taxane resistance, they are extremely prone to the drug if their drug-detoxification strategy is compensated by designing an efficient delivery vehicle.

Magnetic resonance imaging study

Gadolinium, an MRI contrast agent, alters relaxation times of water molecules in tissues where Gd is concentrated after oral or intravenous administration. Theranostic application of non-targeted and folate-targeted NEs were evaluated by injecting 0.072 mmoles/kg of Gd and evaluating tumor accumulation at various time points. Mice were pretreated with pemetrexed to reduce off-target kidney accumulation (Muller et al., 2008). As can be seen in Figure 9(A), folate-targeted NEs showed enhanced contrast compared to non-targeted NEs suggesting active targeting of NEs due to folate modification. Using the tumor region of

interest, the relative T1 signal generated by Gd was used to determine uptake. Folate-targeted NEs and non-targeted NEs showed tumor tissue accumulation over the period of 24 h Figure 9(B). However, clinically used magnevist accumulated in tumor tissues very rapidly and cleared within 5 h Figure 9(B). These results strongly support potential of folate-targeted NEs as a theranostic drug delivery system. Use of such a strategy will provide numerous advantages such as localization of the tumor tissues, determination of drug distribution as well as potential quantification of disease progression.

Discussion

With the clinical advancement and FDA approval of targeted therapies, antibody therapies, antibody-drug conjugate therapies and small-molecule drug conjugates like Endocytes folate-targeted therapies/imaging agents (e.g. vintifolide, EC145), targeting the molecular differences of cancer is no longer fantasy. Targeted nanomedicine is the next evolution of targeted therapies as they can be molecularly “designed” to carry multiple drugs, target disease relevant receptors, and carry diagnostic capabilities suitable of tracking accumulation in diseased tissues. DTX is used to treat ovarian cancer patients as a second line of therapy if patients show resistance to Taxol® or Abraxane® (Paclitaxel formulated in human serum albumin). Often recurrent ovarian cancer patients have been so heavily treated previously that their cancer might be non-responsive to DTX as a second line treatment due to mutations that affects its ability to stabilize tubulin polymerization or over expression of ABC transporters. High expression of one ABC transporter, MDR-1, has been correlated as an independent prognosticator for poor survival for ovarian and renal cancer (Penson et al., 2004; Mignogna et al., 2006). However it is generally believed that either resistance mechanism has the potential to minimize DTX clinical effectiveness, thus a theranostic approach might provide relevant chemical value.

Even with potential for resistance, DTX is a compelling molecule for ovarian cancer patients, *in vitro* DTX is a stronger promoter of tubulin polymerization than paclitaxel partially because of its greater affinity to β-Tublin showing 1.2–2.6 times more cytotoxicity than paclitaxel. However this enhancement in cytotoxicity may also be due to the interaction of docetaxel with BCL-2. BCL-2 is a multidomain antiapoptotic protein that sequesters BAX and BAK proteins, two pro-apoptotic proteins that play a major role in mitochondrial outer membrane permeabilization, a pivotal event in the intrinsic apoptosis pathway (Thanos et al., 2003) DTX and paclitaxel both induce phosphorylation of BCL-2 leading to the release of BAX and BAK, however DTX does so at a concentration 100-fold less than paclitaxel (Sadurni et al., 2005). Clinically there is incomplete cross-resistance, specifically with paclitaxel-resistant breast, lung and ovarian tumors potentially due to different mechanisms of uptake, efflux, or stimulation of apoptosis. Therefore if DTX could be delivered in nanomedicine specifically designed to mitigate reduced uptake, enhanced efflux and apoptosis escape mechanisms associated with multidrug resistance heavily treated recurrent ovarian cancer patients could potentially be treated more effectively than current standard of care second line treatment protocols.

Disease specific targeting is important to deliver higher concentrations of chemotherapy to the tumor and should have the added benefit of limiting side effects by minimizing systemic

distribution. Folate receptor alpha (FR-α) is one of three folate receptor isoforms:, α,β & γ. FR- α is the most widely studied isoform and is a 38 kD glycosyl-phosphatidylinositol-anchored glycoprotein that binds folic acid with a K_d<1 nM and is highly expressed in a number of human tumors including ovarian (>80%), lung (>75%), breast cancer(>60%) renal cell(>65%) and brain, head & neck (Fisher et al., 2008). In normal tissue expression is much lower and limited to kidney tubuli, lung epithelium in the apical cell, the choroid plexus, and placenta (Parker et al., 2005). FR-α over expression is negatively associated with overall survival in ovarian and other cancers; however with >80% of ovarian tumors expressing FR-α it is difficult to power a study appropriately to correlate expression with mortality. As a predictor of response rate to chemotherapy, either complete or partial remission, patients with FR-α greater then median level had a 15-fold higher likelihood of negative response (Toffoli et al., 1997). In the light of correlation with poor clinical outcome we investigated whether targeting FR-α with folate-targeted NE could enhance *in vitro* potency of DTX in taxane sensitive and resistant ovarian cancer cells. FR-α targeting was achieved through the use of a lipidated-version of a folate, a configuration that has demonstrated efficient binding and preferential internalization by folate receptor expressing tumor cells *in vitro*, and tumor xenografts *in vivo* (Goren et al., 2000, Leamon et al., 2003).

In the current study, non-targeted and folate-targeted, DTX-loaded NEs show improved cytotoxicity in both taxanesensitive and taxane-resistant cells. The folate-targeted DTX NE showed a 270-fold increase in cytotoxicity in taxaneresistant cells as compared to DTX alone, a finding that suggests the amount of folate-targeted DTX NE could be reduced significantly and be more effective than current clinically available taxane therapies. Although uptake mechanisms of these NE formulations have yet to be studied in detail, in general NEs fuse with cellular membrane and most likely undergo non-specific transport via phagocytosis. This passive mechanism improved the potency of DTX when compared to DMSO solubilized DTX *in vitro*. However greater potency was observed when the NE was functionalized with folate to facilitate specific uptake via folate receptor-mediated endocytosis. Both these mechanisms, i.e. passive lipid membrane fusion or receptor-mediated endocytosis, mitigated taxane-resistance associated with taxane efflux out of the cell. Delivery via endocytosis appears to protect DTX from ABC transporter mediated drug efflux mechanisms and enhance apoptosis. The remarkable increase in potency of DTX in folate-targeted NEs should be a benefit to ovarian cancer therapy and also potentially limit toxic side effects. For example, less DTX could be used to overcome taxane resistance for patients that have shown resistance to Taxol® or Abraxane®.

Cancer stem cells (CSCs) have recently been shown to preferentially proliferate when treated with platinum and taxane therapies and are implicated in recurrent ovarian cancer which is multidrug resistant (Joo et al., 2013). Our investigation appears to be especially important for recurrent ovarian cancers which might be derived from CSCs which express ABC transporters. Our results indicate that using the folate receptor to deliver DTX could mitigate drug efflux and mitigated some apoptotic escape mechanisms CSCs initiate to survive second line therapies. Perhaps this is through improved phosphorylation of BCL-2 and the release of the proapoptotic proteins BAX and BAK (Sadurni et al., 2005). If this is potentially the case then using a folate-targeted DTX nanoemulsions as a second line

therapy for folate positive recurrent ovarian cancer could improve outcomes and potentially reduce burden of using a toxic drug that provides little efficacy. Additionally, folate-targeted DTX-NEs could be dosed less frequently while still achieving efficacy and reducing the long-term chemotherapeutic burden to the body. Another reason to encapsulate DTX in a folate-targeted NE is that this nanomedicine design might limit systemic toxicities associated with current DTX formulations particularly bone marrow suppression, neutropenia, renal and hypersensitivity. Our studies showed that DTX could be sequestered at high concentrations in the lipid core of a stable folate-targeted NE with a size between 130–150 nm in diameter. This size range is still capable of taking advantage of the EPR effect and active targeting but avoids clearance by the kidney which clears nanomedicines with a diameter <5 nm.

Normally clinical diagnosis of therapeutic efficacy takes a significant amount of time to ascertain, but for patients suffering with recurrent ovarian cancer time is critically important. A delivery vehicle that can inform the physician of drug uptake by a tumor in a relatively short time period post administration and in a non-invasive manner might be a diagnostic attribute that is advantageous for improving care. The NE created for this study was designed as a theranostic capable of simultaneously imaging and targeting drug delivery to folate receptor-positive ovarian tumors. Our NEs were functionalized with Gd-DTPA-PE chelate to track particle uptake by MRI detection (Ganta et al., 2014a). This design with the Gd-chelate residing on the outer surface of the NE provides a suitable environment for Gd longitudinal relaxivity and generates contrast for suitable for clinical MRI. Thus, potentially providing the physician with a visualization method of therapy uptake and potentially improved monitoring of disease progression in recurrent ovarian cancer patients. The NE formulations had comparable magnetic relaxation times *in vitro* comparable to clinically relevant Magnevist®. Moreover, folate-targeted NEs showed enhanced contrast in tumors *in vivo* compared to non-targeted NEs or Magnevist®. Such a theranostic NE allows visualization of the DTX pharmacodynamics with the potential to monitor tumor progression. If the MRI contrast enhancement in the tumor is not consistent with enhanced T1 weighted images consistent with Gd-accumulation, clinicians will have the opportunity to adjust the dosing regimens or change therapies if the theranostic NE appears not to be efficacious.

Overall, this study demonstrates that the theranostic properties of a folate-targeted DTX nanomedicine should be advantageous for the treatment of folate receptor-positive ovarian cancer. As most ovarian cancers will eventually become multidrug resistant we show that targeted delivery of DTX using the folate receptor is capable of overcoming taxane-resistance. The diagnostic potential of the NE is designed for direct monitoring of nanomedicine uptake and has potential for monitoring disease progression. While further preclinical efficacy, imaging and toxicology investigations are required to confirm and translate this theranostic nanomedicine, the potential of its medical utility based on the initial results is promising for folate receptor positive, multidrug-resistant ovarian cancer.

Conclusions

We developed a novel theranostic that delivers DTX by receptor mediated endocytosis that shows enhanced cytotoxicity capable of overcoming ABC transporter mediated taxane resistance. The diagnostic capability of the targeted nanomedicine shows enhanced contrast for prolonged period of time compared to clinically relevant MRI contrast agent Magnevist® in SKOV3 tumor-bearing mice. Our studies indicate that this novel nanomedicine demonstrates significant potential to treat MDR cancers that eventually develop in most ovarian cancer patients. This potentially clinically relevant nanomedicine for MDR cancer was designed to carry DTX in the lipid core of the NE composed of GRAS grade excipients suitable for parenteral administration. DTX encapsulated in a non-targeted NE was more potent than DTX dissolved in DMSO in *in vitro* cytotoxicity assays. However, encapsulation of DTX in a folate-targeted NE enhanced the potency in SKOV3 ovarian cancer cells but significantly increased the potency in taxane resistant SKOV3TR ovarian cancer cells.

The multifunctionality of this novel folate-targeted, Gd annotated, DTX loaded NE formulation demonstrate that clinically relevant capabilities to track drug distribution, evade multidrug resistant mechanisms and potentially mitigate free drug induced systemic toxicity can be designed into nanomedicines. With regards to multidrug resistance mechanisms, e.g. reduced drug uptake, enhanced drug efflux, and escape from apoptosis, the design of this nanomedicine mitigates each of them as shown, by increased caspase 3/7 activity and cytotoxicity. The results indicate the potential for a new class of DTX therapies to treat not only DTX MDR ovarian cancer, but other cancers where taxane therapy is standard of care.

Acknowledgments

We would like to thank Mary Elizabeth Schwartz, Susan Riley Keyes, Allison Morse, Rupa Sawant, Philip Heisler, and Keri Forbringer for assistance with the manuscripts preparation.

References

Clogston JD, Patri AK. Detecting and measuring free gadolinium in nanoparticles for MRI imaging. Methods Mol Biol. 2011; 697:101–8. [PubMed: 21116958]

Ersoy H, Rybicki FJ. Biochemical safety profiles of gadolinium-based extracellular contrast agents and nephrogenic systemic fibrosis. Journal of Magnetic Resonance Imaging: JMRI. 2007; 26:1190–7. [PubMed: 17969161]

Fisher RE, Siegel BA, Edell SL, et al. Exploratory study of 99mTc-EC20 imaging for identifying patients with folate receptor-positive solid tumors. J Nuclear Med. 2008; 49:899–906.

Ganta S, Singh A, Patel NR, et al. Development of EGFR-targeted nanoemulsion for imaging and novel platinum therapy of ovarian cancer. Pharm Res. 2014a

Ganta, S.; Talekar, M.; Singh, A., et al. AAPS PharmSci Tech. 2014b. Nanoemulsions in translational research-opportunities and challenges in targeted cancer therapy.

Goren D, Horowitz AT, Tzemach D, et al. Nuclear delivery of doxorubicin via folate-targeted liposomes with bypass of multidrug-resistance efflux pump. Clin Cancer Res. 2000; 6:1949–57. [PubMed: 10815920]

Grant CW, Karlik S, Florio E. A liposomal MRI contrast agent: phosphatidylethanolamine-DTPA. Magn Reson Med. 1989; 11:236–43. [PubMed: 2779414]

Joo WD, Visintin I, Mor G. Targeted cancer therapy – are the days of systemic chemotherapy numbered? Maturitas. 2013; 76:308–14. [PubMed: 24128673]

Kelly RJ, Draper D, Chen CC, et al. A pharmacodynamic study of docetaxel in combination with the P-glycoprotein antagonist tariquidar (XR9576) in patients with lung, ovarian, and cervical cancer. Clin Cancer Res. 2011; 17:569–80. [PubMed: 21081657]

Lachman, L.; Liebermann, HA.; Kanig, JL. The Theory and practice of industrial pharmacy. Philadelphia: Lea & Febiger; 1986.

Leamon CP. Folate-targeted drug strategies for the treatment of cancer. Curr Opin Investig Drugs. 2008; 9:1277–86.

Leamon CP, Cooper SR, Hardee GE. Folate-liposome-mediated antisense oligodeoxynucleotide targeting to cancer cells: evaluation in vitro and in vivo. Bioconjug Chem. 2003; 14:738–47. [PubMed: 12862426]

Levchenko TS, Rammohan R, Lukyanov AN, et al. Liposome clearance in mice: the effect of a separate and combined presence of surface charge and polymer coating. Int J Pharm. 2002; 240:95–102. [PubMed: 12062505]

Li J, Sausville EA, Klein PJ, et al. Clinical pharmacokinetics and exposure-toxicity relationship of a folate-Vinca alkaloid conjugate EC145 in cancer patients. J Clin Pharmacol. 2009; 49:1467–76. [PubMed: 19837906]

Mignogna C, Staibano S, Altieri V, et al. Prognostic significance of multidrug-resistance protein (MDR-1) in renal clear cell carcinomas: a five year follow-up analysis. BMC Cancer. 2006; 6:293. [PubMed: 17177989]

Muller C, Schibli R, Krenning EP, De Jong M. Pemetrexed improves tumor selectivity of 111In-DTPA-folate in mice with folate receptor-positive ovarian cancer. J Nucl Med. 2008; 49:623–9. [PubMed: 18344429]

Parker N, Turk MJ, Westrick E, et al. Folate receptor expression in carcinomas and normal tissues determined by a quantitative radioligand binding assay. Anal Biochem. 2005; 338:284–93. [PubMed: 15745749]

Penson RT, Oliva E, Skates SJ, et al. Expression of multidrug resistance-1 protein inversely correlates with paclitaxel response and survival in ovarian cancer patients: a study in serial samples. Gynecol Oncol. 2004; 93:98–106. [PubMed: 15047220]

Pusztai L, Wagner P, Ibrahim N, et al. Phase II study of tariquidar, a selective P-glycoprotein inhibitor, in patients with chemotherapy-resistant, advanced breast carcinoma. Cancer. 2005; 104:682–91. [PubMed: 15986399]

Rose DP, Connolly JM. Omega-3 fatty acids as cancer chemopreventive agents. Pharmacol Ther. 1999; 83:217–44. [PubMed: 10576293]

Ruff P, Vorobiof DA, Jordaan JP, et al. A randomized, placebo-controlled, double-blind phase 2 study of docetaxel compared to docetaxel plus zosuquidar (LY335979) in women with metastatic or locally recurrent breast cancer who have received one prior chemotherapy regimen. Cancer Chemother Pharmacol. 2009; 64:763–8. [PubMed: 19241078]

Sadurni N, Solans C, Azemar N, et al. Studies on the formation of O/W nano-emulsions, by low-energy emulsification methods, suitable for pharmaceutical applications. Eur J Pharm Sci. 2005; 26:438–45. [PubMed: 16153811]

Seiden MV, Swenerton KD, Matulonis U, et al. A phase II study of the MDR inhibitor biricodar (INCEL, VX-710) and paclitaxel in women with advanced ovarian cancer refractory to paclitaxel therapy. Gynecol Oncol. 2002; 86:302–10. [PubMed: 12217752]

Spannuth WA, Sood AK, Coleman RL. Farletuzumab in epithelial ovarian carcinoma. Expert Opin Biol Ther. 2010; 10:431–7. [PubMed: 20092424]

Sudimack J, Lee RJ. Targeted drug delivery via the folate receptor. Adv Drug Deliv Rev. 2000; 41:147–62. [PubMed: 10699311]

Thanos CG, Liu Z, Goddard M, et al. Enhancing the oral bioavailability of the poorly soluble drug dicumarol with a bioadhesive polymer. J Pharm Sci. 2003; 92:1677–89. [PubMed: 12884254]

Toffoli G, Cernigoi C, Russo A, et al. Overexpression of folate binding protein in ovarian cancers. Int J Cancer. 1997; 74:193–8. [PubMed: 9133455]

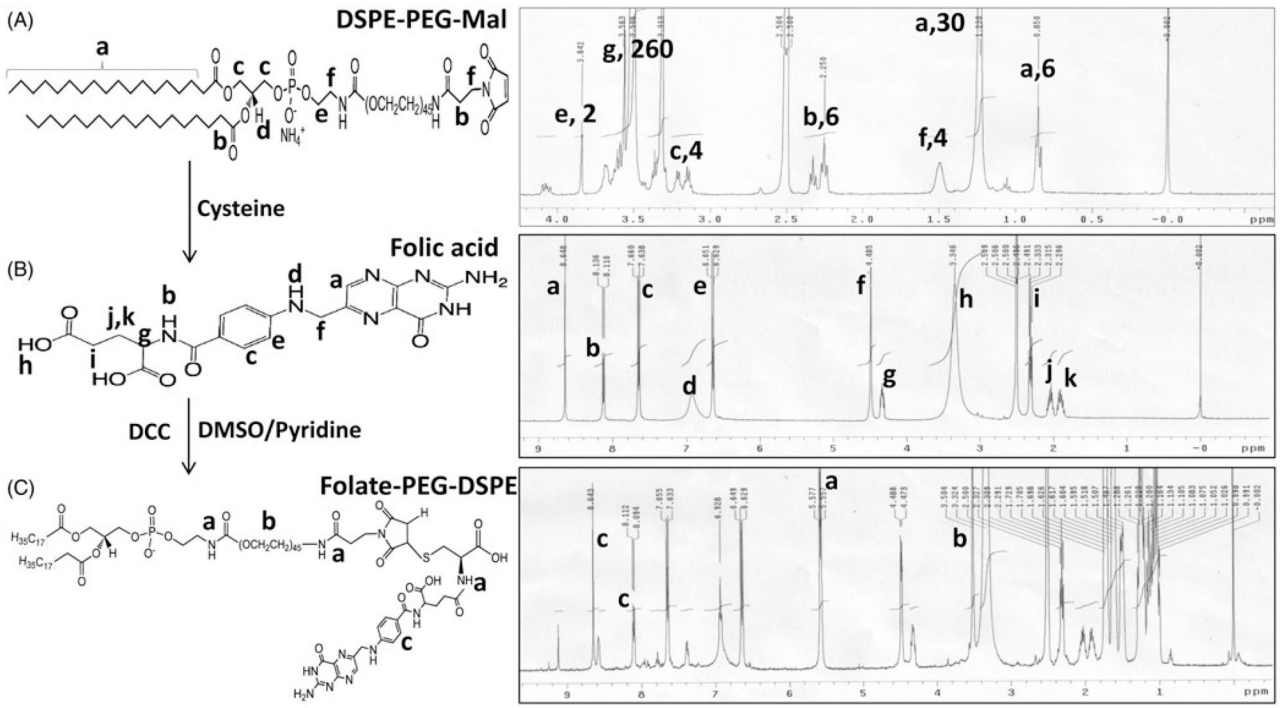

Figure 1.
Scheme of folate-PEG-DSPE synthesis and structural confirmation using NMR spectra.

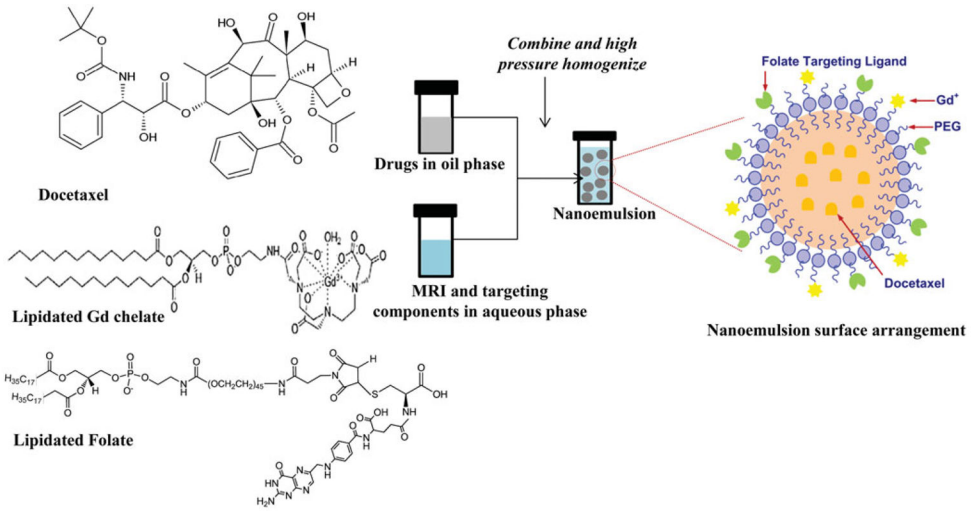

Figure 2.

Schematic showing encapsulation of DTX into lipid core of NE and its surface is modified with Gd and folate for MRI functionality and targeting, respectively.

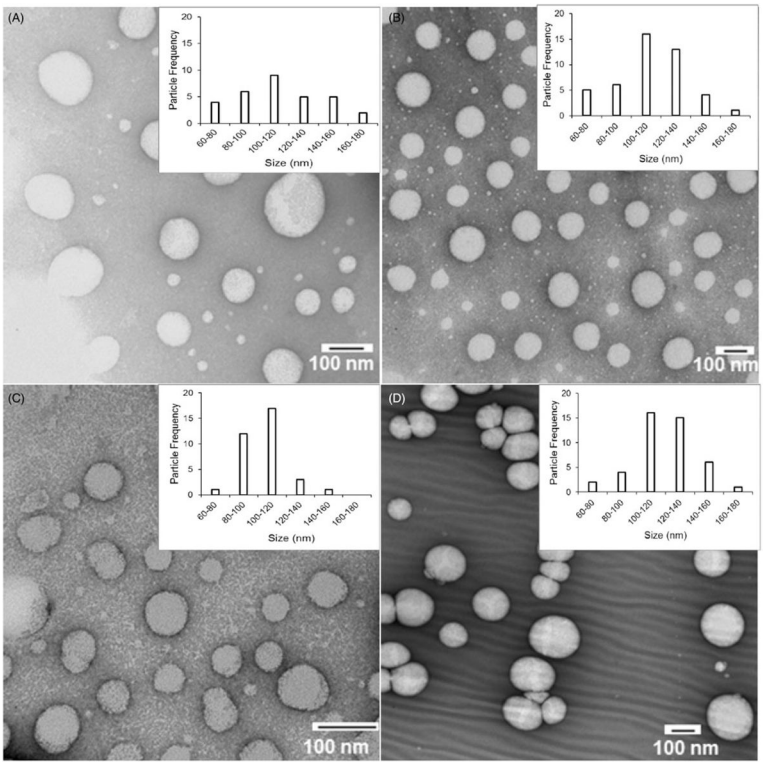

Figure 3.

TEM Transmission electron microscopy images of NE formulations (A) Blank NE (NT), (B) Blank NE (Folate), (C) DTX-NE (NT), and (D) DTX-NE (Folate).

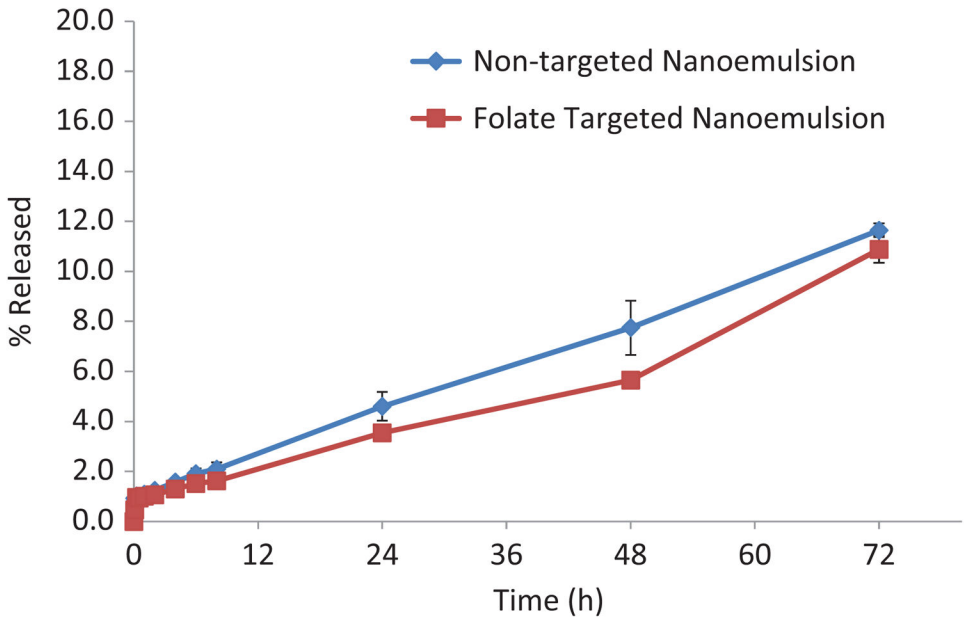

Figure 4.

DTX release from the non-targeted and folate targeted NE formulations in PBS (pH 7.4) containing 0.5% Tween 80 at 37 °C. The data are shown as mean±SD (*n*=3).

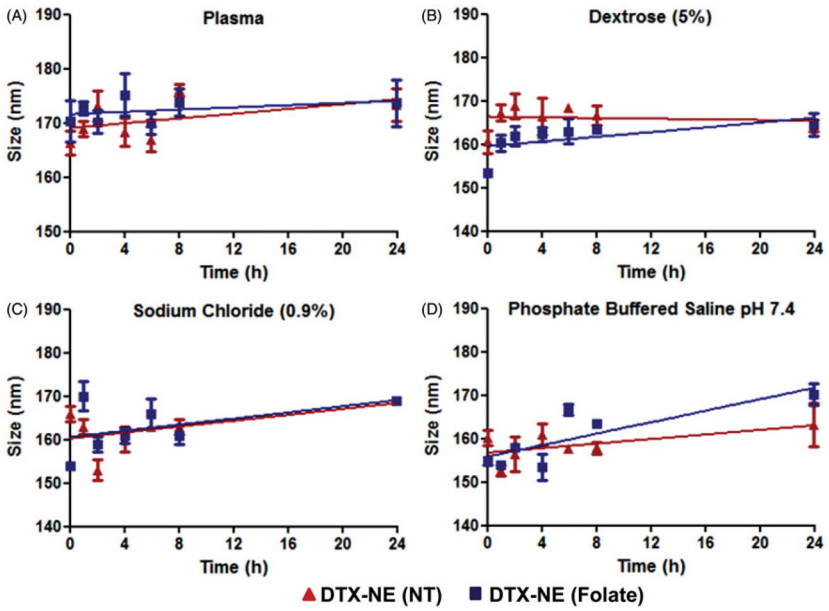

Figure 5.

Physical stability of DTX containing non-targeted and folate targeted NE formulations upon 90% dilution in dog plasma, parenteral infusion fluids (5% dextrose and 0.9% sodium chloride) and phosphate buffered saline. The data are shown as mean ±SD (*n*=3).

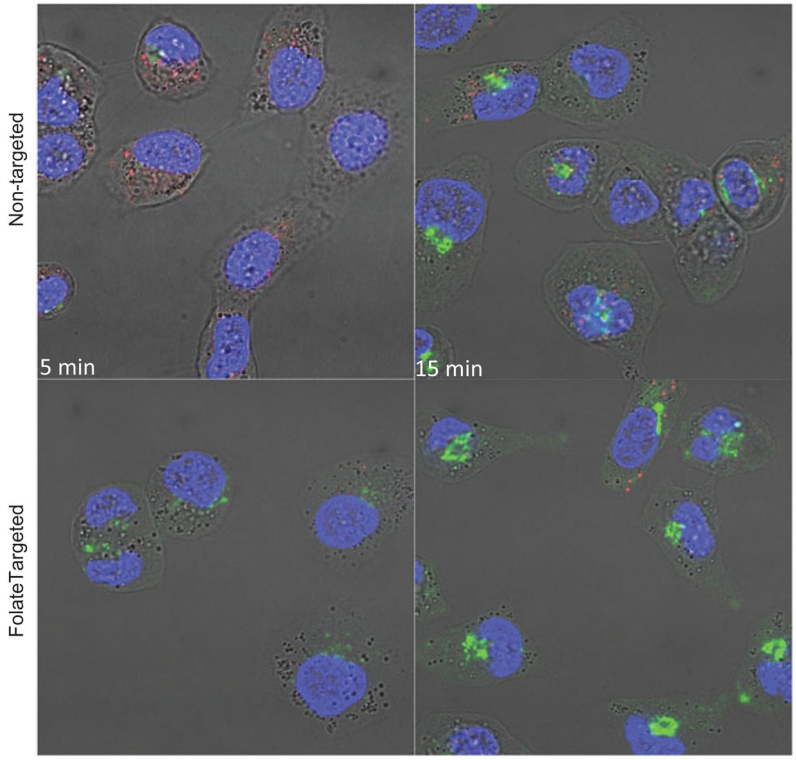

Figure 6.

Fluorescent microscopy images showing uptake of NBD-ceramide (green) containing non-targeted and folate targeted NEs in SKOV3 cells. Lyso Tracker (red) and DAPI (blue) were used to stain lysosomes and nucleus respectively and to monitor the co-localization of NE in SKOV3 cells.

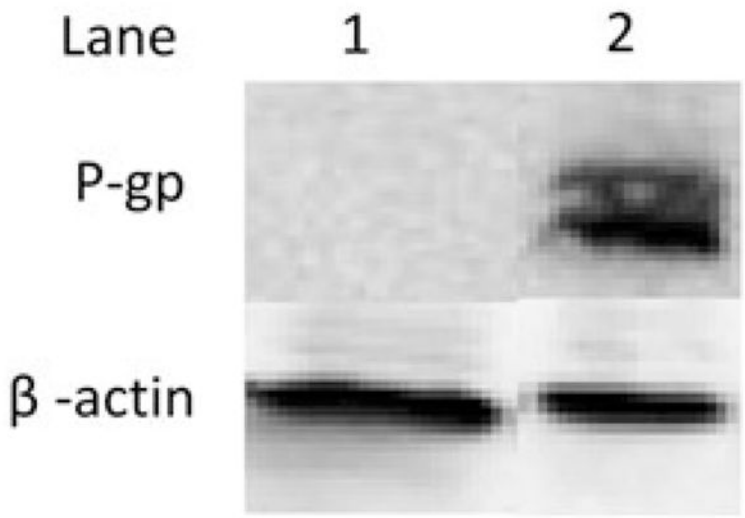

Figure 7.

P-glycoprotein expression in SKOV3, SKOV3TR cells using western blot analysis. Lane 1: SKOV3 cells (20 μg protein lysate), Lane 2: SKOV3TR cells (20 μg protein lysate). β-actin was used as a loading control.

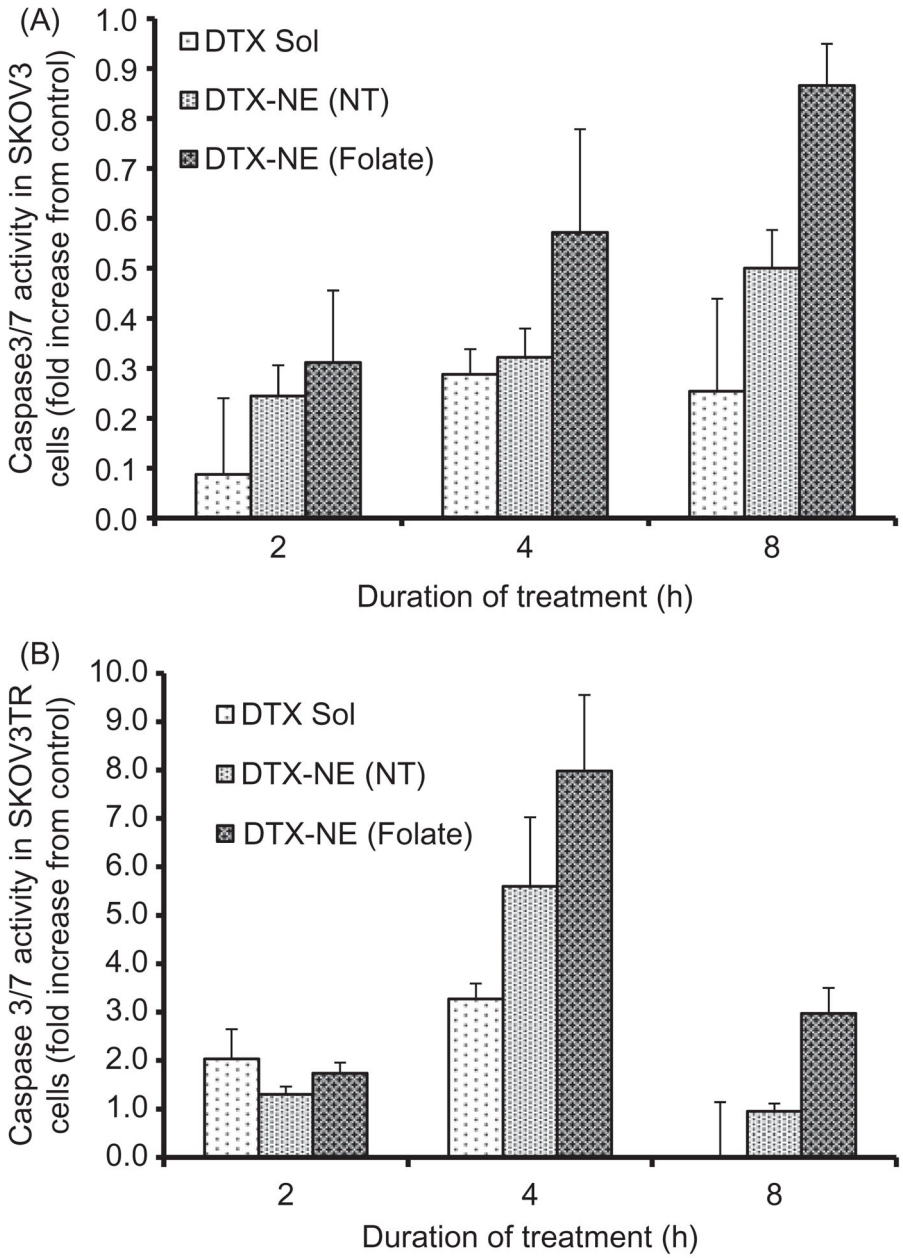

Figure 8.

Caspase 3/7 activity assay in (A) SKOV3 and (B) SKOVTR cells treated with DTX in non-targeted NE (DTX-NE (NT)) and folate targeted NE (DTX-NE (Folate)), relative to DTX solution (DTX Sol). The data are shown as mean±SD (*n*=2).

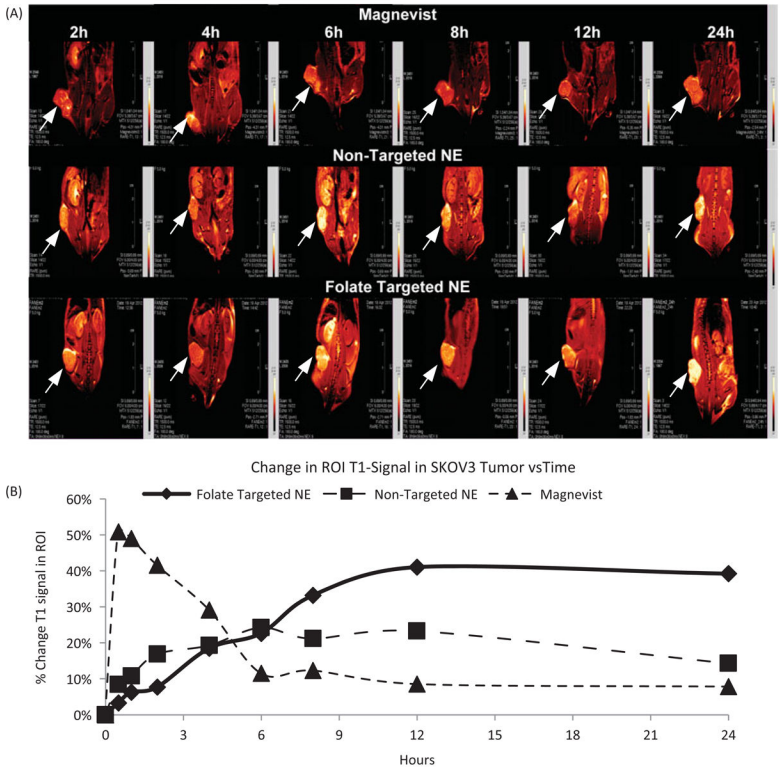

Figure 9.

(A)T1 weighted images and (B) quantitative analysis of % tumor signal versus time of mice bearing subcutaneous SKOV3 tumor xenograft post i.v. injection of magnevist, non-targeted NEs and folate-targeted NEs with pemetrexed treatment at final concentration of Gd at 0.072 mmoles/kg, the data are shown as mean ±SD (*n*=3).

Table 1

Characterization of formulations.

	Hydrodynamic diameter of formulations				
Formulations	**Size (nm)**	**PDI**	**Zeta potential (mV)**	**DTX encapsulation (%)**	**T1 values (msec)**
Blank NE	142±7	0.1	−50±10	–	
Blank NE (folate-targeted)	123±22	0.1	−52±10	–	
DTX-NE (non-targeted)	130±3	0.1	−50±12	100	34.51±13.5
DTX-NE (folate targeted)	135±6	0.06	−54±10	100	79.46±2.63

Magnevist had T1 values of 22.2±0.27. The values are shown as Avg±SD, *n*=3.

Table 2

Drug release kinetics.

	Zero order		First order		Higuchi equation	
Formulation	**R^2**	**K_0**	**R^2**	**K_1**	**R^2**	**K_2**
Non-targeted NE	0.9929	0.341765	0.9128	0.035466	0.9439	2.805284
Folate-targeted NE	0.9716	0.301923	0.9053	0.036157	0.8862	2.427362

Table 3

IC_{50} values.

Formulation	SKOV3	Fold improvement	SKOV3TR	Fold improvement
DTX solution	1.0±1.3nM	1.00	27 000±4050nM	1.00
DTX non-targeted NE	0.5±1.2nM	2.00	6800±1400nM	3.97
DTX folate-targeted NE	0.3±1.2nM	3.33	100±12 nM	270